Achieving High Levels of Selectivity for Kinase Inhibitors

Laurent Schio and Herve Minoux

Contents

Abstract Kinase inhibitors have emerged over the last two decades as one of the most prolific therapeutic classes of agents to reach clinical trials and to obtain marketing approval, mainly for oncology. We describe here the methodologies that we performed for hit and lead finding in the context of four internal projects to identify selective inhibitors for development or preclinical pharmacological evaluation.

Keywords Kinase inhibitors, Ligands, Oncology, Protein conformations, Selectivity, Targeted therapy

---

L. Schio (✉) and H. Minoux
Integrated Drug Discovery, Sanofi, Vitry-sur-Seine, France
e-mail: Laurent.Schio@sanofi.com

1   Introduction

It is estimated that 5% of the human genome is dedicated to protein phosphorylation. 518 different human kinases have been identified and clustered in sub-groups depending on substrate specificity and sequence similarity, but overall these enzymes catalyze the same biochemical reaction, the transfer of a phosphate group to a serine, threonine, or tyrosine residue [1]. From a pharmaceutical standpoint, there is huge evidence that kinase activities are deregulated in a broad range of diseases (cancer, inflammation, Parkinson, etc.) (https://www.cellsignal.com/contents/resources-reference-tables/kinase-disease-associations/science-tables-kinase-disease) which has triggered over the last decades a massive interest in identifying and developing selective kinase inhibitors.

Cancer treatment is definitely the most important therapeutic domain where kinases inhibitors have found their application, and today approximately 50 small molecular weight kinase drugs have received marketing approval by the FDA, in addition to a dozen of monoclonal antibodies directed mainly against the human epidermal growth factor receptor kinase family (EGFR, HER2) [2, 3].

The first generation of marketed drugs (Gleevec, Sutent, Sprycel, etc.) [4] exhibited multi-kinase inhibition profiles, supporting the paradigm that better efficacy would be achieved by multi-cellular pathway blockade and giving the opportunity to register the same drug in different indications (e.g., Gleevec launched in 2001 for the treatment of patients with Philadelphia chromosome-positive chronic myeloid leukemia (CML) and in 2002 for the treatment of patients with Kit-positive unresectable and/or metastatic malignant gastrointestinal stromal tumor (GIST)) [5].

The development of the targeted therapy paradigm in oncology [6, 7] as well as the clinical demand for much better tolerated treatments has conducted research programs in pharmaceutical companies towards the discovery of selective to exquisite kinase inhibitors [8–10].

Successful development of drugs targeting specific deregulated cellular signaling pathways via selective inhibition of one targeted kinase (e.g., MEK) [11] or of oncogenic mutants (e.g., EGFR DM, V600E BRAF) [12] has been achieved recently [13, 14].

However, in the 1990s, when the first 3D crystal structure of a kinase (PKA) [15] was reported, a largely believed myth emerged that it would be impossible to develop selective and potent protein or lipid kinase inhibitors by targeting the ATP binding site due to a priori lack of specificity and high level of sequence similarity across the kinome. In mid-2019, more than 6,000 human protein kinases and more than 160 human lipid kinase 3D structures were deposited in the PDB (https://www.rcsb.org/). Thorough analyses of apo-structures vs ATP analog or ligand bound co-structures have revealed general modes of kinase activation [16, 17], including those behind oncogenic mutations [18–20], as well as subtle specific interactions in the active site and several preferred conformations (DFG-in, DFG-out, and α helix-out) [21, 22].
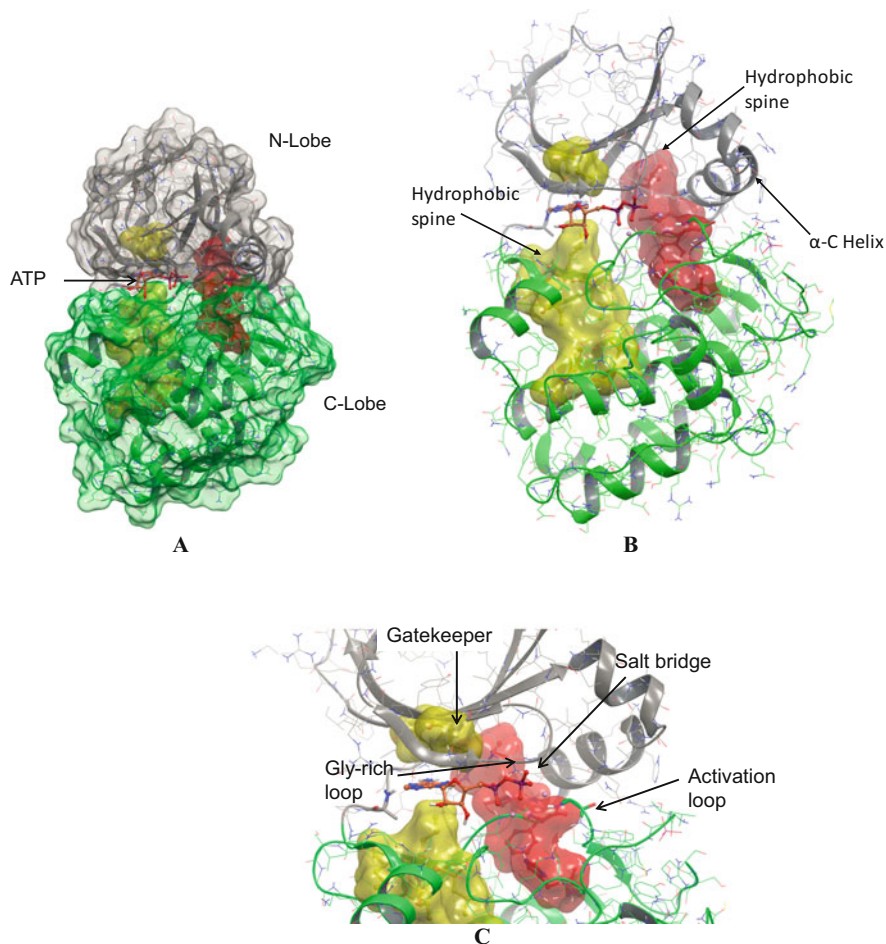
Fig. 1 General view of Aurora A kinase; (**a**) N-lobe is colored in grey and C-lobe in green. ATP is represented in ball and stick in its pocket at the interface between the two lobes; (**b**) surfaces of the residues forming the hydrophobic spines of Aurora A are colored in red and yellow. (**c**) Positions of the glycine-rich loop, activation loop, and gatekeeper (GK) residues are indicated

Figure 1a–c represents a general view of a kinase (Aurora A) for which key motifs and residues for activation and activity are highlighted:

Figure 2a, b describes a simplified view of a kinase active site where key residues and motifs for protein activation are depicted. These residues correspond to the general model of kinase activation reported by Taylor and coworkers [16]. The "$^{\text{N-lobe}}$lysine" is the residue which is involved in a salt bridge with usually a glutamate residue from the αC- helix ("$^{\alpha\text{C}}$glutamate") in a competent DFG-in conformation, whereas the "$^{\text{cat}}$lysine" from the catalytic loop interacts with the γ-phosphate of ATP to assist its transfer to the kinase substrate. The "$^{\text{phospho}}$residue"
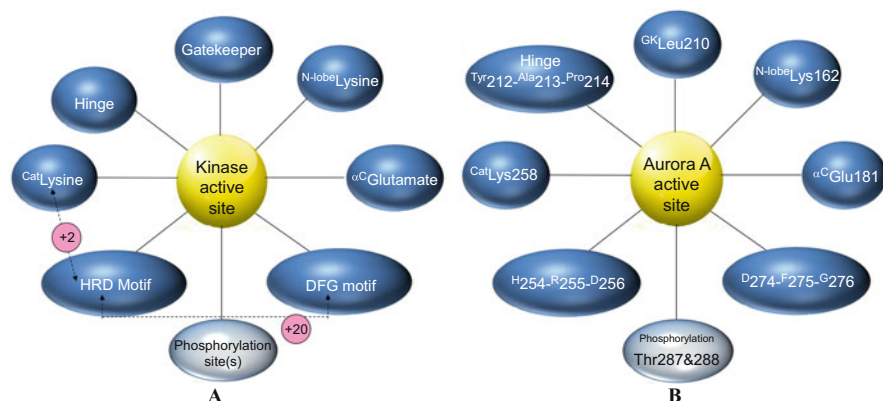
Fig. 2 (**a**) General kinase motif mapping (KMM), (**b**) KMM of Aurora A

corresponds to the phosphorylated residue in the activation loop. In general, the distances between these groups are conserved (numbers mentioned in pink in Fig. 2a). Figure 2b describes the ATP site of Aurora A in this schematic representation (Kinase Motif Map; KMM).

Recently, a chemogenetic study based on kinase sequence similarity and structure-activity relationship (SAR) analysis underlined 16 *privileged* residues in the active site that are recurrently involved in kinase protein stabilization and ligand binding [23]. In our ATP active site representation applied to Aurora A, the privileged motifs involved in protein ligand interactions are indicated in yellow and those involved in controlling the active vs inactive conformations balance in magenta (Fig. 3). The gatekeeper residue (Leu210) as well as two hinge residues (Tyr212, Pro214) are also privileged residues for ligand specificity. Interestingly, this analysis underlines the importance of hydrophobic residues which stabilize by packing the kinase active conformation and forming the so-called hydrophobic spine (Leu196 – $^{\alpha C}$Gln185 – Phe275 – Leu208 – His254) [24].

It was originally thought that DFG-out related inhibitors would be more selective as this conformation has not been observed across the all kinome and has been publicized by the clinical success of Gleevec [25, 26]. Moreover this class of inhibitors is expected to be less impacted by micromolar concentrations of ATP in cells as they have shown non-competitive binding vs ATP in biochemical assays compared to active conformation directed ligands (DGF-in inhibitors) [8]. This selectivity trend has not been confirmed globally with DFG-out kinase inhibitors [27], but it has been shown that α-C helix-out inhibitors revealed exquisite selectivity profiles (e.g., MEK and HER2 inhibitors) [28, 29] albeit potentially at the expand of potency against oncogenic mutants, for which the inactive conformations are disfavored (e.g., lapatinib) [30].

We will describe in this chapter what were the medicinal chemistry strategies undertaken in our group to identify and develop selective kinase inhibitors for four
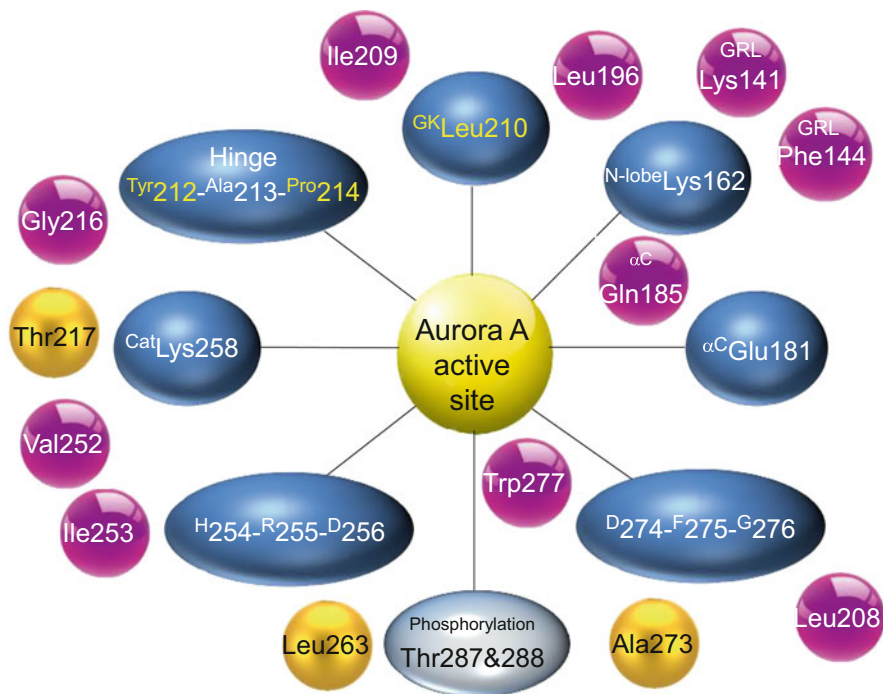
Fig. 3 KMM of Aurora A with *privileged* residues indicated

oncology projects, leveraging interactions with specific protein residues, active and inactive conformations, and stable/unstable water molecules in the ATP cleft.

2 Discovery of an Exquisite Selective Aurora Inhibitor as Neo-Cytotoxic Agent

The Aurora kinases exist as three isoforms (A, B, C), belong to the serine/threonine protein kinase family, and regulate cell division. The Aurora kinases are expressed and active predominantly during the G2/M phase of the cell cycle [31]. These kinases are involved in the control of the centrosome and nuclear cycles and have essential functions in mitotic processes such as chromosome condensation, spindle dynamics, kinetochore-microtubule interactions, chromosome orientation, and establishment of the metaphase plate. Each Aurora isoform has its own function during mitosis in line with its specific distinct localization, namely, the centrosomes and spindle poles for Aurora A and the centromeres and spindle mid-zone for Aurora B. Aurora A and Aurora B kinases are expressed in all dividing cells, whereas Aurora C kinase is mainly expressed in the testes and plays a role in spermatogenesis [32–34].
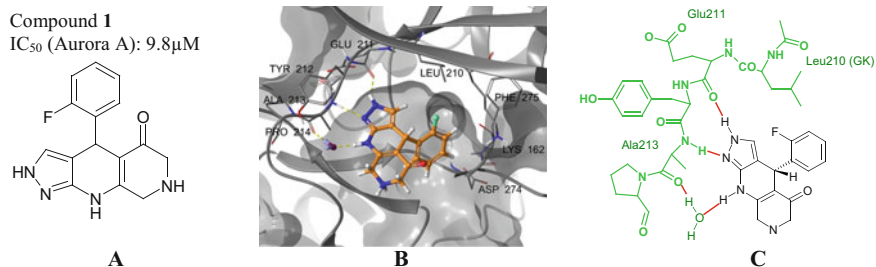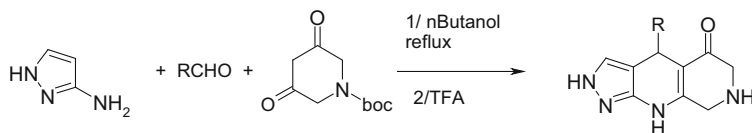
Compound **1**
IC$_{50}$ (Aurora A): 9.8μM

A   **B**   **C**

Fig. 4 Inhibition of Aurora A by compound **1**; (**a**) 2D structure of compound **1** and its activity on Aurora A; (**b**) X-ray structure of compound **1** (displayed with carbon atoms in orange) bound to Aurora A; surface of Aurora A ATP-pocket is displayed in grey. (**c**) 2D scheme of compound **1** (black) bound to Aurora A and a bridging water molecule (green). Hydrogen-bond are represented as red lines

The Aurora kinases have been found aberrantly expressed in several solid tumors (bladder, breast, gastro-intestinal, liver, pancreatic, and thyroid) and in hematopoietic malignancies such as acute myeloid leukemia (AML), chronic myeloid leukemia (CML), multiple myeloma (MM) and lymphomas. Moreover, Aurora A and B overexpression has been associated with poor prognosis in ovarian carcinoma and non-small cell lung cancer, respectively. Also, *Aurora A* gene has been detected amplified in 50% colon, 25% ovarian, 12% breast, more than 90% pancreatic, and 50% bladder carcinomas. In tumors, Aurora A overexpression correlates with aneuploidy and Aurora B with genomic instability [34–36].

These observations have lent interest to this family of kinases as potential drug targets for the development of new anti-cancer therapies [37]. At the time we embarked in a discovery program to identify novel Aurora inhibitors, several compounds with various levels of selectivity either with respect to Aurora A vs Aurora B or regarding off-target kinases were advancing into preclinical phases or early clinical trials [38]. Our objective was to design and develop exquisitely selective inhibitors of the Aurora proteins in order to assess the intrinsic efficacy and tolerance of such neo-cytotoxic agents in relevant pharmacological tumor models.

Based on a pharmacophoric model established from publicly reported X-ray structures of Aurora A, about a million of internal compounds were screened in silico for their ability to match at least partially the model with the requirement to potentially interact with the hinge residues (e.g., Ala 213, Fig. 2b) [39]. After several runs of docking studies and probabilistic analysis, a set of 3,500 compounds was selected for assessing in vitro their inhibition potency of the Aurora kinase activity at 10 μM. Among the few chemical series which emerged in this assay with decent activity, our interest rapidly focused on the 1,2,4,6,7,8-hexahydro-5H-pyrazolo [3,4-b]-[1,7]naphthyridin-5 series represented by compound **1** which displayed hints of selectivity when tested at 20 μM against a panel of kinases (Fig. 4a). This chemical class was selected for further exploration despite modest affinity of **1** on Aurora A but considering a satisfactory ligand efficiency (LE = 0.33) and a

Scheme 1 Synthesis of a library of analogs of compound 1, using a one-step three-component Hantzsch reaction

Compound **2**
IC$_{50}$ (Aurora A) = 300nM
IC$_{50}$ (Hela) >10μM

Compound **3**
IC$_{50}$ (Aurora A) = 100nM
IC$_{50}$ (Hela) >10μM

Compound **4**
IC$_{50}$ (Aurora A) = 18nM
IC$_{50}$ (Hela) = 300nM

Compound **5**
IC$_{50}$ (Aurora A) = 9nM
IC$_{50}$ (Hela) = 15nM

SAR156497
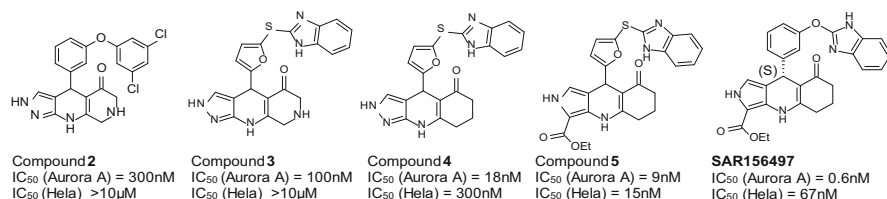IC$_{50}$ (Aurora A) = 0.6nM
IC$_{50}$ (Hela) = 67nM

Fig. 5 2D structures of compounds from the tricyclic series, with their inhibitory activity on Aurora A as well as their activity in HeLa cell proliferation assay

promising selectivity profile. Co-crystallization trials were promptly initiated in order to define the binding mode of this rather unusual class of kinase inhibitors.

The 3D structure elucidation of **1** in complex with Aurora A protein highlighted the molecule in the S-configuration bound in the ATP site (Fig. 4b) and interacting with the hinge residue Ala213 via the central ring NH through a bridging water molecule and via the pyrazole moiety. Compound **1** developed an additional hydrogen bond with Glu211, at the vicinity of the gatekeeper residue, again with the pyrazole (Fig. 4c). Looking at the conformation of the complex, the DFG moiety was found positioned "mid-in / mid-out," the phenylalanine side chain of Phe275 being oriented toward the N-lobe and in contact with the αC-helix, the latter being shifted compared to a canonical active conformation, and the salt bridge between the [Nlobe]Lys162 and the [αC-helix]Glu181 being disrupted. Therefore, the observed conformation of the complex with **1** was considered as non-competent or inactive [40].

As this chemical series is readily accessible in a one-step three-component Hantzsch reaction, a library of analogs of **1** was produced in a racemic form using various aldehydes (Scheme 1).

Extension of the aryl moiety on the tricyclic core turned out to produce more active derivatives (e.g., compounds **2** and **3** in Fig. 5) displaying also enhanced selectivity for Aurora A (IC$_{50}$ > 10 μM against a panel of about 30 kinases tested). Co-crystallized in Aurora A, compound **3** exhibiting the S-configuration adopted a similar binding mode compared to **1** at least regarding the tricyclic core in interactions with the hinge. However, the DFG motif was unequivocally oriented in the *in* configuration and the thio-benzimidazole group expanded into the hydrophobic back pocket behind the gatekeeper residue (Leu210). Interestingly, the benzimidazole moiety was engaged in a double interaction with [Nlobe]Lys162 and [αC-helix]Gln185, a privileged residue, preventing the salt bridge formation (Fig. 6a) and the close
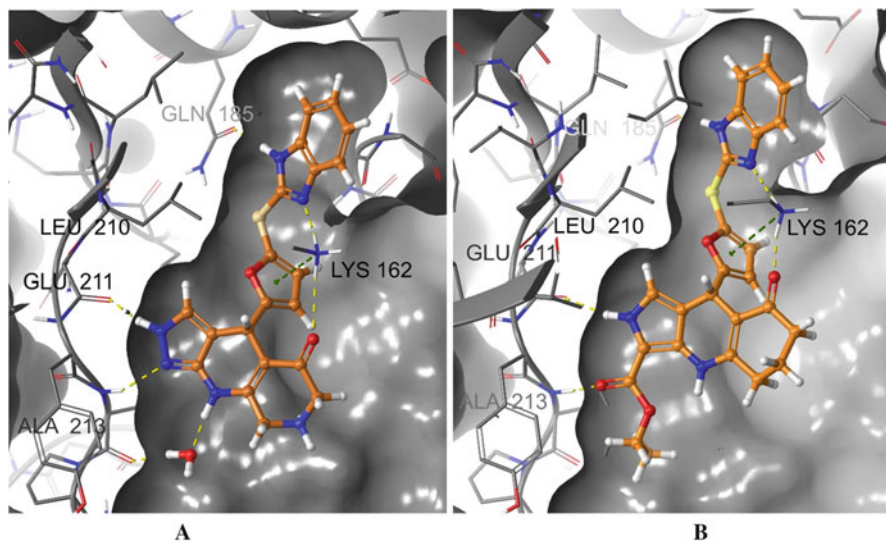
Fig. 6 (**a**) Compound **3** in Aurora A. (**b**) Compound (+)-**5** in Aurora A (IC$_{50}$ = 4 nM)

contact of the αC-helix to the ATP cleft. This conformation called *αC-helix out* has been also reported to be the very specific inhibitory mechanism of lapatinib against Her2 and EGFR [30].

Despite decent potency vs Aurora A, compound **3** was devoid of any anti-proliferative activity when tested against a limited panel of cancer cell lines. Subsequent gain of affinity was obtained by removing the nitrogen atom in the pyridinone ring despite structural evidence of its involvement in an H-bond with a water molecule in the binding pocket. The resulting molecule (compound **4**, Fig. 5), a low double digit nanomolar Aurora A inhibitor, blocked Hela proliferation at 300 nM (IC$_{50}$). Compound **4** exhibited also a potent affinity for Aurora B (IC$_{50}$ = 5 nM) and otherwise was shown to be totally inactive against other kinases tested (except Tie2, IC$_{50}$ = 3 μM).

In a second round of chemical optimization, the pyrazole moiety was modified, and the 2-ethoxycarbonyl-pyrrole group emerged as being the most productive substitution in terms of anti-proliferative potency in Hela cells (compound **5**, Fig. 5), whereas biochemical activity was only slightly improved compared to **4**. Compound **5** was resolved by chiral chromatography, and the dextrogyre enantiomer (+)-**5** (S-configuration) was identified as the active substance of the racemic mixture: Aurora A, IC$_{50}$ = 4 nM; Aurora B, IC$_{50}$ = 2 nM; and Hela cells, IC$_{50}$ = 2 nM (the levogyre enantiomer was inactive). The binding mode of (+)-5 in Aurora A was characterized to be very similar to the one observed for three but with two major differences. First, the hinge Ala213 NH was directly involved in an H-bond with the carbonyl of the carboxylate moiety (no water bridge). Second, the ^{Nlobe}Lys162 interaction with the benzimidazole-N was stabilized via a second interaction with a water molecule. Compound (+)-**5** was measured equipotent on the three Aurora

isoforms (Aurora C, $IC_{50} = 4$ nM) but otherwise totally inactive ($IC_{50} > 10$ μM) on all other kinases tested. Our hypothesis to explain such high and rare level of selectivity shared by compounds **4**, **5**, and other analogs made in the series relies first on the fact that the *αC-helix out* conformation is not accessible to a broad ensemble of kinases for ligands/inhibitors [26]. Key determinants which would drive the occurrence of this inactive kinase conformation remain unclear but may be related to the gatekeeper size and the packing forces developed along the hydrophobic spine [41]. In the case of compounds **3** and **5** in complex with Aurora A, the benzimidazole core interacts with a glutamine residue (Gln185) localized in position "$^{αC-helix}$glutamate + 4," a reported privileged residue/position. We analyzed among the kinome the occurrence of a glutamine in this position and found it rare at 2%.

Compound (+)-**5** was able to inhibit both Aurora A and Histone-H3 phosphorylation in HCT116 cell lines ($IC_{50} = 70$ and 10 nM, respectively), two relevant biomarkers of Aurora A and B inhibition to monitor pharmacodynamic modulation in vitro and in tumor models. Moreover, this compound displayed low nanomolar anti-proliferative activities against a large panel of cell lines and exhibited no toxicity on quiescent PBL cells providing evidence that targeting Aurora isoforms triggers specific and lethal effects on cancer cell lines but no damage on non-proliferative normal cells. Drug-likeness liabilities of compound (+)-**5** (Cyp inhibition, exposure in rats, hepatocyte clearance, and PDE3 inhibition) were then optimized to give rise to **SAR156497**, a molecule which has demonstrated a narrow therapeutic window when tested in a murine model of human colon adenocarcinoma xenograft [39].

3 Development of a Selective MET Kinase Inhibitor Active Against Oncogenic Mutants

MET is a tyrosine kinase which is involved in embryonic development and wound healing in normal cells. MET acts as a transmembrane receptor which is stimulated by the hepatocyte growth factor (HGF) inducing *in fine* cell proliferation, migration, and invasion [42]. Abnormal activation of the HGF-MET pathway has been frequently observed in human cancers in particular in solid tumors where MET protein is usually overexpressed [43]. Moreover, *MET* gene has been found amplified in 5–12% of gastric carcinoma, 2–13% of lung cancers, and 4–12% of colon-rectal carcinoma. Oncogenic mutations of the *MET* gene have been observed in multiple human cancer types (hepatocellular, papillary renal cell and head and neck carcinoma, etc.) leading to protein structure changes and activation [44]. Five major mutants of the kinase domain have been expressed in our group and tested for catalytic activity and have exhibited a four- to five-time enhancement of catalytic activity (Kcat) compared to the wild-type protein (internal data – Fig. 7a for mutation locations). Whereas Y1230H, Y1235D, L1195V, and H1094Y are mutated residues located at the vicinity of the ATP binding site (Figure 7b for the KMM representation), M1250T is remote to the ATP binding cleft and may influence catalytic
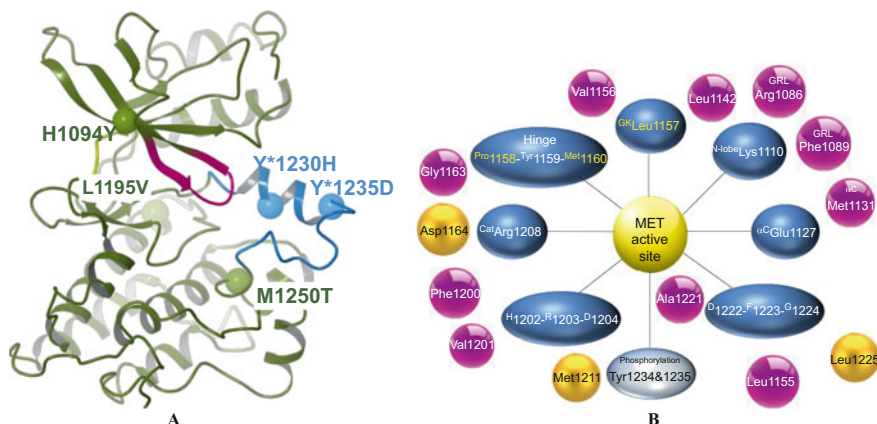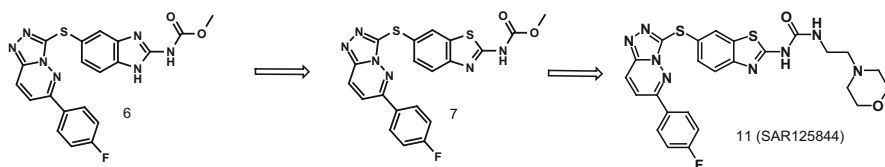
Fig. 7 (**a**, **b**) KMM of MET

Scheme 2 From hit to candidate

activity by allosteric effects [45]. MET activation has been reported to promote tumor initiation, metastasis, angiogenesis, and resistance to diverse therapies, including against anti-EGFR cancer agents [46].

To date, there is no selective MET inhibitor that is FDA-approved. Crizotinib (Xalkori) was originally tested in MET deregulated lung cancer patients but obtained its primary registration as ALK inhibitor in ALK translocation-positive NSCLC [47]. Several orally bioavailable MET tyrosine kinase inhibitors are currently in advanced clinical trials [48]. We will describe thereafter the discovery process which allowed the identification of **SAR125844**, an exquisite selective MET inhibitor investigated in phase II clinical trials for MET-amplified NSCLC patients (https:// clinicaltrials.gov/ct2/show/NCT01391533).

From a two-step screen of a limited set of in house compounds, a hit (**cpd 6,** Scheme 2) was identified with low nanomolar potency against wild-type (WT) MET ($IC_{50} = 10$ nM), but this molecule also exhibited a marked affinity for tubulin, a major constituent of the cytoskeleton involved in DNA segregation, leading then to off-target cytotoxicity in non-MET-dependent tumor cell lines [49, 50].

Compound **6** displayed otherwise no activity ($IC_{50} > 10$ μM) against a panel of kinases tested, in particular CDK9 a key player in cell cycle regulation and gene transcription [51]. This potent and selective MET inhibitor, obtained in a rather straightforward   manner   by   compound   collection   screen,   exhibited   the
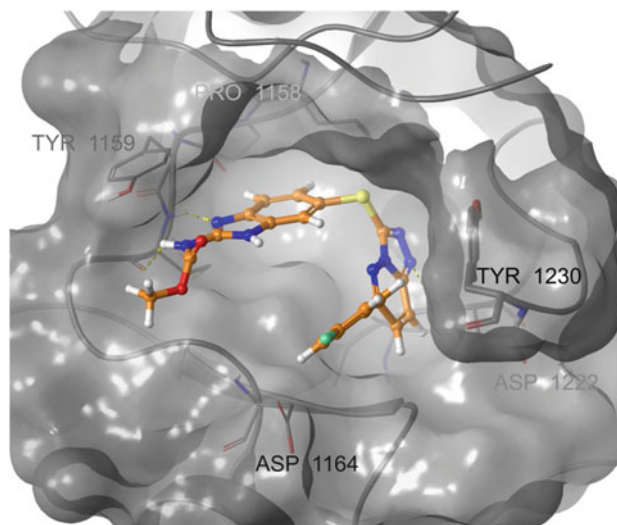
Fig. 8 Compound **6** (carbon atoms colored in orange) in MET ATP cleft

triazolopyridazine core, a chemical group introduced in this benzimidazole series in a historical anti-helminthic project developed in the 1980s in the company. Compound **6** could be co-crystallized in MET, and the 3D-structure of the complex was assessed. Structural analysis revealed compound **6** bound into the ATP pocket, developing in total three H-bonds, two with a hinge residue (Met1160), and one with the main-chain nitrogen atom of Asp1222 (DFG motif) via a nitrogen atom of the triazolopyridazine moiety. Moreover, the triazolopyridazine ring made a specific π-π interaction with Tyr1230 of the activation loop found in a non-competent conformation (Fig. 8). This specific binding mode involving Tyr1230 is believed to be a major driver of the selectivity for MET displayed by this chemical series and others [52]. Moreover, MET does not respect the general mode of kinase activation described by Taylor [16] since the salt bridge between Lys1110 and Glu1127 of the α-C Helix is disrupted (or not formed) as observed in the 3D structure of MET with a non-hydrolysable ATP analog (AMP-PNP) [53]. Instead α-C Helix Glu1127 inter-acts with Arg1227 of the A-loop which opens up an additional hydrophobic pocket exploited by ARQ197, a selective inhibitor of MET auto-phosphorylation [54]. In contrary to ARQ197, compound **6** did not disrupt the hydrophobic spine of MET formed by a stacking cascade of Leu1142, [αHelix]Met1131, [DFG]Phe1223, and [HRD]His1202, but the α-C Helix was somewhat further displaced compared to the structure with AMP-PNP. The reported binding mode of **6** is shared with crizotinib, JNJ-38877605, SGX-523, and AMG-337, and other members of the so-called type I class of MET inhibitors [52].

The switch from the benzimidazole chemical scaffold to the benzothiazole core (compound **7**) dialed out affinity for tubulin and positive outcome in the Ames assay.

Fig. 9 2D representation of the common scaffold shared by compounds reported in Table 1
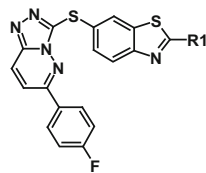
Subsequent incorporation of various chemical groups (amides, amines, carbamates, and ureas) in position 2 (R1, Fig. 9) of the benzothiazole scaffold gave rise to more potent compounds not only against WT MET but also vs the different mutants tested (Table 1).

In general, reduced affinity was measured vs the mutants tested compared to the WT protein which tolerated a broad range of substituents in this 2-position. Introduction of the morpholino-ethyl urea moiety led to the most active derivative of this sub-series in particular against the clinically relevant Y1230H mutant (cpd **11**; IC_{50} = 204 nM).
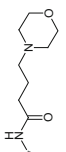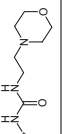
Attempts to co-crystallize compound **11** in WT MET turned out to be unsuccessful, but 3D co-structures were otherwise readily obtained with the selected MET mutants. Structural analysis of the three complexes with **11** revealed a very similar conformation (Fig. 10a), the ligand developing four conserved major hydrogen bonds in the ATP binding site, three with Met1160 and Lys1161 of the hinge, and one with Asp1222 of the DFG motif (Fig. 10b). However, the activation loop segment bearing residue 1,230 was not visible in any structure generated. Our hypothesis at least regarding Y1230H was that the strong π- π interaction observed in the WT protein between Tyr1230 and **11** was affected in the case of His1230 preventing stabilization of the activation loop and leading to reduced affinity for this mutant.

Potency against the Y1230H mutant could be significantly enhanced by modification of the substituent attached to the triazolopyridazine core. In particular replacement of the para-fluorophenyl moiety by a thiophene afforded the most potent derivative (**12,** Fig. 11a) vs Y1230H mutant (IC_{50} = 23 nM) which could be co-crystallized in the mutant protein. 3D co-structure analysis detected a clear positioning of the histidine residue (Fig. 11b), and the triazolopyridazine plane of **12** was twisted outward by ~20° compared to its position in the crystal structure of compound **6** in WT protein (Fig. 11c) [50].

High potency of **12** against MET Y1230H mutant could then be rationalized by more productive hydrophobic contacts between H1230 and the triazolopyridazine-thiophene segment which is planar compared to the skewed nature of the triazolopyridazine-p-fluorophenyl one.

Compound **11** was eventually selected as a candidate for development with respect to its eADME properties, its overall PK profile, and observed pharmacological effects in MET driven tumor models [55]. SAR125844 (**11**) displayed a favorable tolerance profile and preliminary evidence of antitumor activity in phase I

Table 1 Biochemical and cellular activities of compounds 8, 9, 10 and 11

Compound	R1	P-MET WT IC$_{50}$ (nM)	MKN-45 proliferation IC$_{50}$ (nM)	L1195V IC$_{50}$ (nM)	M1250T IC$_{50}$ (nM)	Y1230H IC$_{50}$ (nM)	logD (pH 7.4)
8	NH$_2$	10	81	9,000	245	>10,000	>4.6
9		3	7	61	13	883	4.7
10		6	12	318	93	1,172	4.3
11 (SAR125844)		4	7	64	6	204	4.2

P-MET WT: IC50 measured using protein phosphorylation in a biochemical assay. MKN-45 Proliferation: IC50 measured in proliferation assay using MKN-45 cell line. L1195V, M1250T and Y1230H: IC50 measured using corresponding MET mutants in a biochemical assay. logD measured experimentally by high performance liquid chromatography (HPLC) (Xterra MS C18 column)
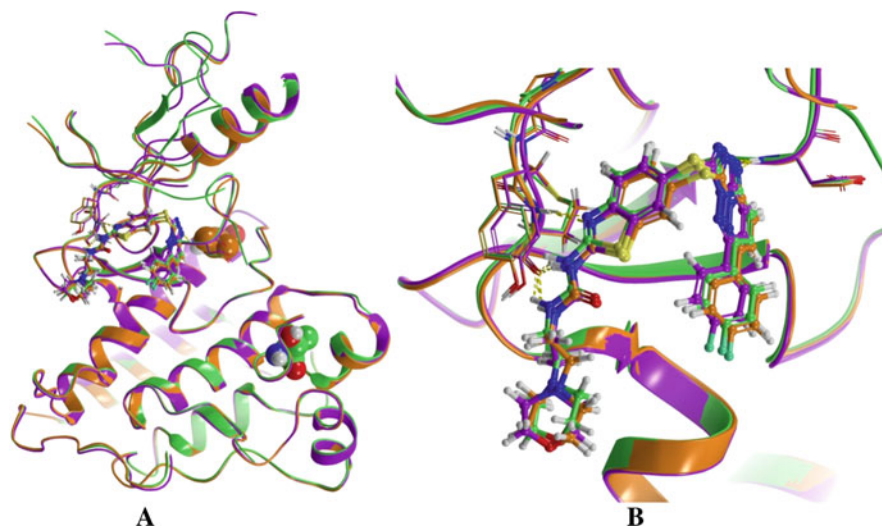
Fig. 10 Superimposition of co-crystal complexes of compound **11** bound to MET Y1230H (purple), MET L1195V (orange), and MET M1250T (green). (**a**): Mutated residues are displayed as CPK, when visible. (**b**): Focus on the ATP-binding pocket, highlighting a conserved binding conformation of compound **11** in the three mutant proteins
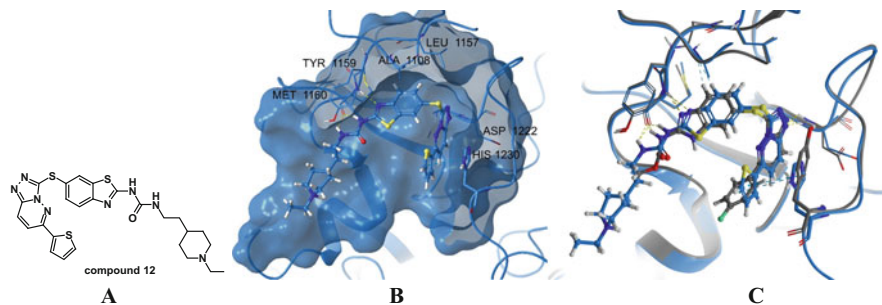

Fig. 11 (**a**) 2D structure of compound **12**. (**b**) Co-crystal of compound **12** bound to the ATP-binding pocket of MET Y1230H. (**c**) Superimposition of co-crystal complexes of compound **6** bound to MET WT (carbon atoms colored in grey) and of compound **12** bound to MET Y1230H (carbon atoms colored in blue). Residue 1,230 is on the right-hand part of the picture

patients which triggered the decision to evaluate the drug in a phase II clinical trial in MET-amplified NSCLC patients (NCT02435121) [56].
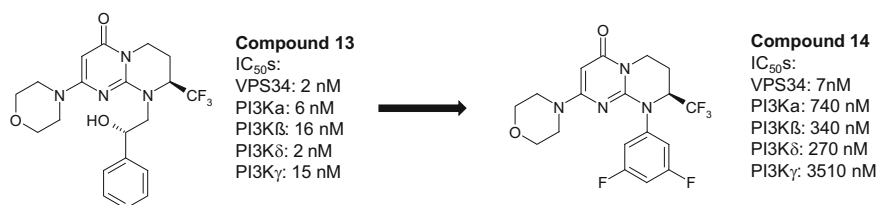
4 Design of Specific VPS34 Inhibitors for Autophagy Blockade in Tumors

VPS34 (also known as PIK3C3) is a lipid kinase of the class III PI3K (phosphoinositide 3-kinases) isoform which specifically catalyzes the phosphorylation of phosphatidylinositol (PtdIns) generating (PtdIns)3P [57]. VPS34 is the catalytic subunit of different complexes which associates the regulatory subunit Vps15 (also known as p150) for activity and several accessory subunits. Vps15 is myristoylated allowing the VPS34 protein complex to be anchored to intracellular membranes. Membrane-bound PtdIns3P binds to proteins which are involved in the formation of autophagosomes and participate also in endosomal trafficking from early to late endosomes [58, 59].

VPS34 plays an active role in the autophagy process by which cells adapt to protect themselves from metabolic stresses and hypoxic conditions. Autophagy is thought to be a process by which cancer cells develop resistance against chemotherapy and radiotherapy treatments. VPS34 has hence emerged as a new promising approach for cancer treatment as a single agent or in combination and recently as a target for insulin resistance in type 2 diabetes [60].

At the time we embarked in a drug discovery project in this field, no selective VPS34 inhibitors were known in the literature [61], and research studies were reported with pan PI3K inhibitors reflecting the high similarity in sequences between classes of PI3K (I-III) [62]. Using a phenotypic screen [63], the pyrimidinone hit **13** was identified with regard to its ability to inhibit (PtdIns)3P production in a transfected Hela cell line (IC_{50}, 1 nM). However, this molecule displayed a poor selective profile, being equally potent vs VPS34 than vs the four class I PI3K isoforms (Scheme 3) [64].

Further analog testing in the pyrimidinone series highlighted compound **14** as a more interesting starting point for chemical optimization, keeping the same level of potency vs VPS34 but with improved selectivity. Compound **14** could be co-crystallized in VPS34 protein, and the 3D structure of the complex was elucidated with satisfactory resolution (3 Å-Fig. 12a). Compound **14** interacted in the ATP site in a DFG-in conformation and developed key interactions with Phe684 (H-bond with the hinge), the N-lobe Lys636, and privileged residues, namely, Asp644 of the

Compound 13
IC_{50}s:
VPS34: 2 nM
PI3Ka: 6 nM
PI3Kß: 16 nM
PI3Kδ: 2 nM
PI3Kγ: 15 nM

Compound 14
IC_{50}s:
VPS34: 7nM
PI3Ka: 740 nM
PI3Kß: 340 nM
PI3Kδ: 270 nM
PI3Kγ: 3510 nM

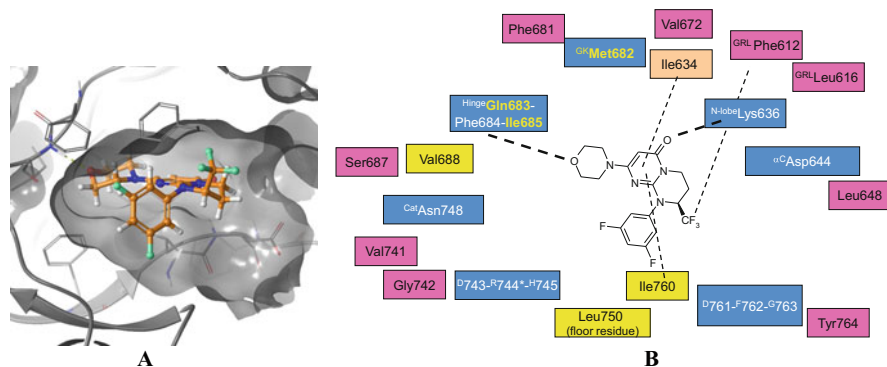**Scheme 3** Selectivity profile of compounds **13** and **14**

Fig. 12 (**a**) Compound **14** (carbon atoms colored in orange) in VPS34 ATP cleft, displaying a DFG-in conformation of the protein kinase. (**b**) Kinase motif map of VPS34 ATP site with cpd **14**. Of note, in VPS34 as in PI3Ks, the HRD motif is inverted (DRH), the [cat]Lys is mutated in [cat]Asn, and the αC-Glu replaced by a αC-Asp. The P-loop is poor in glycine residues therefore will not be referred as Gly-rich loop
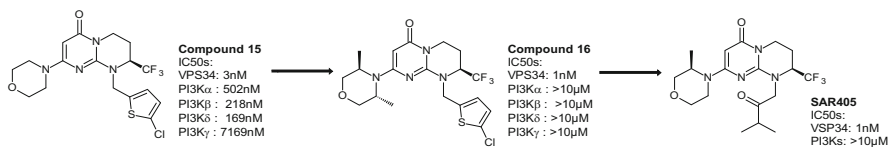
Scheme 4 From hit to lead

αC-helix, the floor residue Leu750, the DFG-1 residue Ile760, and Phe612 in the P-loop (Fig. 12b).

Despite a significant impact of the lateral N-side chain structure on selectivity, it was not possible to totally dial out affinity vs PI3Kδ in particular via chemical modifications at this position only (compound **14** and **15** profiles in Schemes 3 and 4). Therefore, we turned our attention to the morpholine hinge binding motif environment. There are few residues which differ in the active site of VPS34 vs the class I PI3Ks. In particular in the hinge region, both the gatekeeper and floor residues are mutated (Met vs Ile and Leu vs Met, respectively) offering potential levers for selectivity [64]. The introduction of two methyl groups on the morpholine gave rise to compound **16** exhibiting high potency on VPS34 and exquisite selectivity vs the PI3Ks and mTOR (Scheme 4).

Compound **16** was able to co-crystallize in VPS34, and a 3D structure segment is displayed in Fig. 13a. The shape of **16** positioned in the published X-ray structure of PI3Kδ (PDB code, 2WXL, Fig. 13b) highlighted potential steric clashes near Ile825 (GK) on one hand and with Met900 (floor residue) on the other hand.

Multi-parametric optimization eventually led to the discovery of **SAR405** (Scheme 4) which affected vesicle trafficking and autophagy in cell lines and demonstrated sustained inhibition of the autophagy process in a murine tumor
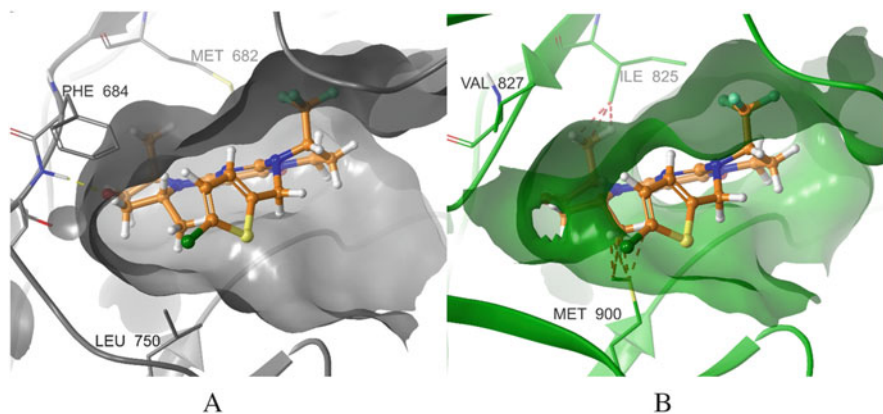
Fig. 13 (**a**) X-ray structure of compound **16** (displayed with carbon atoms in orange) bound to VPS34; surface of VPS34 ATP-binding pocket is displayed in grey. (**b**) Superimposition of co-crystal complex of compound 1**6** (carbon atoms colored in orange) bound to VPS34 and of X-ray structure of PI3Kδ (PDB code 2WXL; protein carbon atoms and surface colored in green). VPS34 protein is not displayed. Steric clashes between compound **16** and residues Ile825 and Met900 of PI3Kδ are depicted as red dotted lines

xenografted model [64, 65]. Moreover **SAR405** synergized with mTOR inhibitor everolimus for cell proliferation inhibition in renal carcinoma models [66].

5 PI3Kβ Inhibitor: Leveraging Water Molecules in the Active Site for Selectivity Enhancement

The class I PI3K lipid kinases are key mediators of the Akt pathway which they contribute to activate by phosphorylating the phosphatidylinositol-4,5-bisphosphate (PIP2) on the 3-position to form phosphatidylinositol-3,4,5-trisphosphate (PIP3) [67]. The class I PI3Ks comprises four isoforms PI3Kα, PI3Kβ, PI3Kδ, and PI3Kγ which share high level of sequence identity. Whereas PI3Kα, PI3Kβ, and PI3Kδ (subclass IA members) can be activated by receptor tyrosine kinases or GPCRs, PI3Kγ the single member of the subclass IB is activated by GPCRs. In addition, class IA PI3Ks are heterodimer enzymes composed of a p85 regulatory subunit and a p110 catalytic subunit harboring the kinase domain [68]. PIP3 then recruits PDK1 and Akt (PKB) at the membrane surface which allows phosphate transfer from PDK1 to Akt (on Thr308). Additional phosphorylation of Akt on Ser473 by mTORC2 results in full activation of Akt triggering downstream upregulation of effectors and elicits cellular processes as proliferation, angiogenesis, survival, and metabolism [69]. In normal cells, the Akt pathway is tightly regulated by the phosphatase and TENsin homologue (PTEN) which dephosphorylates PIP3 back into PIP2. In cancer cells, several activating genetic abnormalities have been detected in the Akt pathway such as gain of function mutations in *PIK3CA* gene, which encodes for the p110α catalytic subunit of PI3Kα, amplification of the *PIK3CA* gene, and deletion of the
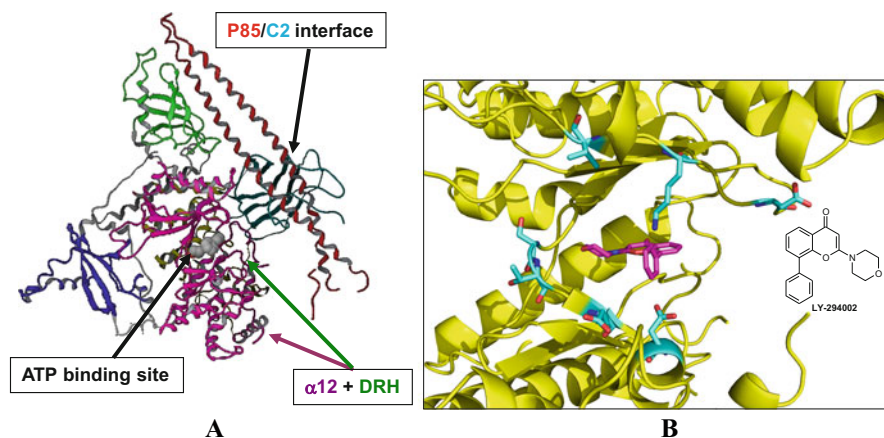
Fig. 14 (**a**) 3D view of p110β /p85 interface. (**b**) LY-294002 docked in PI3Kβ active site (homology model)

tumor suppressor *PTEN* gene. Both *PIK3CA* somatic mutation and *PTEN* deletions are in general mutually exclusive [70]. PTEN-deficient cell lines have been demonstrated to depend on PI3Kβ activity as downregulation of the *PIK3CB* gene by shRNA led to cell growth and tumor growth inhibitions correlated with pAKT inhibition. In those cells, *PIK3CA* gene inhibition induced no effect regarding phosphorylation of AKT 473-residue [71].

As PTEN is deficient in many cancers including the most prevalent ones and those associated with the lowest survival rates (e.g., 23% occurrence in lung, 35% in colon, and 47% in gastric cancers) [72], it was relevant to engage a discovery program to identify selective PI3Kβ inhibitors, expecting a superior safety profile for such agents compared to the generation of pan-PI3K inhibitors which exhibited limiting adverse effects in clinical settings [73].

Our drug discovery strategy was to target the ATP site of PI3Kβ (p110β) and to disregard other approaches such as protein-protein interactions inhibition. The disruption of the p110 β /p85 interface in the activated state of the protein complex via inhibition of the C2 (p110b) /iSH2 (p85) domains interaction [74] (Fig. 14a) was investigated but estimated to be of low probability of success due to computed limited drugability [75].

Sequence similarity analysis of the kinase domains of the four PI3K isoforms revealed that PI3Kβ shares 76% identity with PI3Kδ, its closest isoform. Focusing on the ATP cleft per se, identity reaches 100% with PI3Kα and PI3Kδ. Only few residues differ across the four isoforms and are located at the ATP site entrance (Ser855, Thr856, Glu858, and Asp862) or in the P-loop (Lys777, Asp780, and Val789). These residues are highlighted in the PI3Kβ docking structure established in complex with LY-294002 [76], a well reported and widely used pan-PI3K inhibitor (Fig. 14b).

Kinase	GK	Hinge	Hinge	next to hinge	DFG-1	Floor residue		
				ligand protein interactions				
PI3Kb	Ile851	Glu852	Val854	Glu858	Ile936	Met926		
VPS34	Met682	Gln683	Ile685	Val688	Ile760	Leu750		
				active-inactive conformations control				
Kinase	hinge area	GK area	GK area	GRL	GRL	αHelix	DFG+1	HRD area	HRD area
PI3Kb	Ser857	Val850	Cyst841	Met779	Met783	Leu817	His940	Ile917	Gly918
VPS34	Ser687	Phe681	Val672	Phe612	Leu616	Leu648	Tyr764	Val741	Gly742

Fig. 15 Comparative privileged residues of PI3Kβ vs VPS34. *GRL* glycine-rich loop
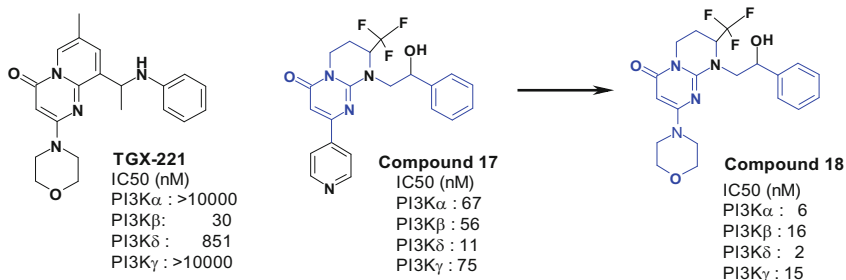

Scheme 5 Hit chemical exploration

It is worth noting that Glu858 is one of the privileged residues [23] of PI3Kβ ("next to hinge" residue) which is mutated in a valine (Val688) in VPS34 (Fig. 15). Overall, PI3Kβ and VPS34 share 27% identity and 40% homology with respect to the nature of these privileged residues (Fig. 15). It was therefore expected to identify PI3Kβ inhibitors with no off-target activity on VPS34 (and vice versa).

Rather than embarking in an ab initio drug design approach for hit finding, we decided to leverage high-throughput screens performed with our in-house compound collection on PI3Kα and PI3Kγ by testing resulting actives on PI3Kβ. Among them, our attention focused on compound **17**, a potent inhibitor of PI3Kβ (IC$_{50}$ = 56 nM) but also vs the other isoforms. Interestingly, compound **17** exhibited structural resemblance with TGX221 a publicly reported PI3Kβ selective inhibitor (Scheme 5). Tested against a panel of kinases, compound **17** showed potency against CDKs in particular and low nanomolar inhibition of VPS34 as a close analog of the afore-mentioned compounds **13–16**. Replacement of the pyridine group on the pyrimidinone scaffold afforded compound **18**, still a pan-PI3K inhibitor but otherwise selective vs the other kinases tested, including the CDKs, VPS34, and mTOR, and except DNA-PK.

Further chemical exploration of this bicyclic pyrimidinone series did not really succeed in gaining selectivity towards PI3Kβ. Fortunately, in an attempt to synthesize the malonate derivative **20**, excess of reagent **19** offered the pyridinone **21** as a by-product which was then modified into anilide **22** to reflect TGX-221 structure (Scheme 6). To our delight, compound **22** turned out to be potent on PI3Kβ and reasonably selective vs PI3Kδ [77].
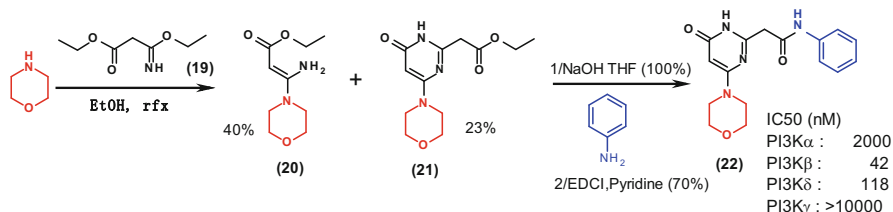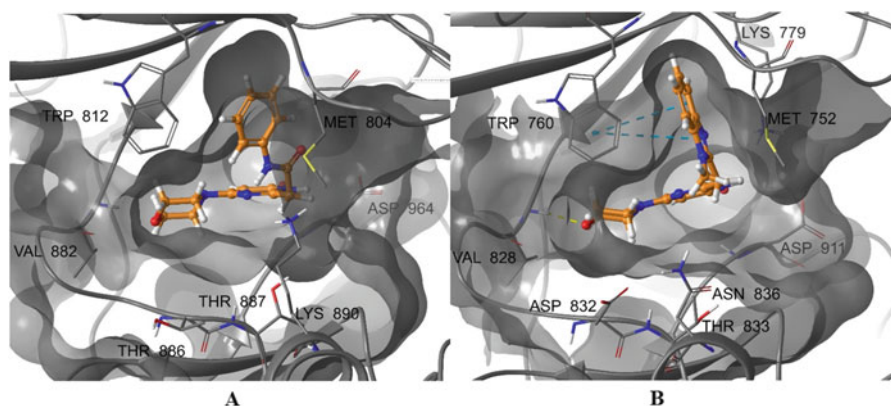
Scheme 6 Chemical synthesis of compound 22

Fig. 16 (**a**) Compound **22** co-crystallized in PI3Kγ. (**b**) Compound **23** co-crystallized in PI3Kδ. Ligand carbon atoms are colored in orange

To rationalize the observed selectivity and potency, compound **22** was co-crystallized in PI3Kγ, which served as structural platform at the time the compound was synthesized, despite no inhibitory activity measured on this isoform ($IC_{50} > 10$ μM). Interestingly compound **22** exhibited a different mode of binding compared to LY-294002, adopting a propeller shape as previously described for the selective PI3Kδ inhibitor PIK-39 in complex also with PI3Kγ despite again no activity on this isoform [78]. In the co-crystal, compound **22** interacted classically with the hinge Val854 NH residue via the morpholine oxygen, but more interestingly the phenyl group was projected towards the P-loop in the so-called selectivity pocket resulting from a movement of Met804 (Fig. 16a), a conserved residue across the PI3Ks.

Compound **22** and other anilide derivatives suffered from lack of in vivo stability due to rapid cleavage of the amide bond. We next generated a series of benzimidazoles derivatives and identified compound **23** as advanced lead for the project [77]. The 3D-structure of compound **23** in complex with PI3Kδ could be obtained and confirmed the binding mode of **22** observed in PI3Kγ. Similarly, the corresponding methionine residue of [γ]Met804 in the P-loop ([δ]Met752) changed its conformation compared to its position in the apo-structure, leaving space for the
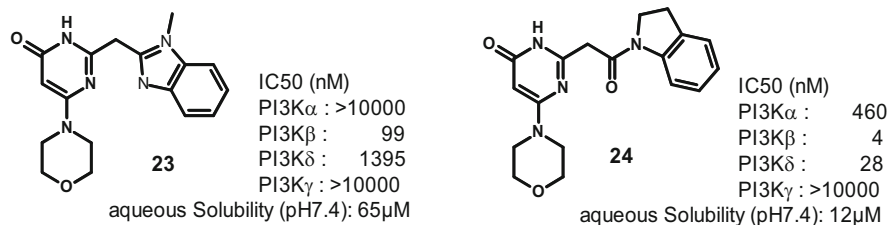
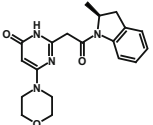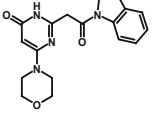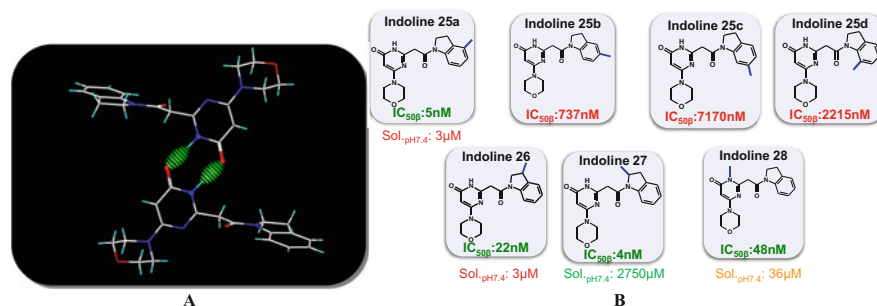**Scheme 7** in vitro profile of compounds **23** vs **24**

Fig. 17 (**a**) X-ray crystal structure of **24**. (**b**) Outcome of the methyl scan approach

methyl-benzimidazole moiety to bind in the created selectivity pocket delineated on the other hand by another conserved residue, namely, Trp760. However limited aqueous solubility and modest on-target potency precluded further development of compound **23** which chemically evolved then towards the more active but still poorly water-soluble pyrrolidine derivative **24** (Scheme 7). Improvement of potency on PI3Kβ for **24** was translated into potent pAkt inhibition in PTEN-deficient PC3 cell line, superior to **23** (IC_{50} = 15 nM vs 65 nM). The indoline **24** structure is associated with a moderate experimental logP (1.4); therefore, the lack of solubility in the thermodynamic conditions tested was attributed to potentially high-energy packing forces in its solid form in line with the high melting point value measured with the produced batch (mp = 285°C).

The X-ray crystal structure of compound **24** was solved from single diffraction data. Crystal packing analysis underlined the formation of dimers via head-to-tail alignments through donor-acceptor N − H···O contacts (2.74 Å) between pyrimidone moieties (Fig. 17a). Close interconnection of molecules was further favored both by indoline π-stacking and indoline/morpholine C − H···π interactions. It was then postulated that solubility in the series could be enhanced by introduction of substituents (e.g., methyl group) which would disrupt such network of inter molecule interactions. We embarked then in methyl scan chemistry approach supported by molecular modeling calculations which highlighted several positions in the **24** chemical structures which would tolerate substitution.

Table 2 Biochemical activities of compounds (R)-27 and (S)-27 on five kinases, in nM

Compound	Structure	PI3Kα (IC$_{50}$)	PI3Kβ (IC$_{50}$)	PI3Kδ (IC$_{50}$)	PI3Kγ (IC$_{50}$)	pAkt inh. PC3 (IC$_{50}$)
(S)-27		1,000	23	468	10,000	49
(R)-27		569	6	6	3,315	12

Methylation of the phenyl ring was tolerated by the PI3Kβ binding site only in position 4 (indoline **25a**, Fig. 17b), but no improvement of solubility was noticed. Methylation of the pyrimidinone core (indoline **28**) was tolerated regarding activity, slightly increased solubility compared to **24**, but this avenue was dismissed since it introduced a metabolic hot spot. Methylation in position 3 had no effect in contrary to position 2 which brought an outstanding improvement of solubility. The racemic indoline **27** was separated into its two pure enantiomers, and another unexpected finding was obtained: the (R)-isomer-**27** was found equipotent on PI3Kβ and PI3Kδ, whereas the (S)-isomer-27 retained selectivity vs PI3Kδ but at the expense of activity on PI3Kβ (Table 2).

Whereas PI3Kβ had been refractory to intensive efforts deployed in house and elsewhere to find conditions and constructs in order to obtain crystals of the kinase domain [74], we finally succeeded and reported for the first time the X-ray structure solved at 2.8 Å of a propeller shaped ligand ((S)-**27**) in complex with p110β (http://www.rcsb.org/structure/4BFR). Moreover (S)-**27** could be also co-crystalized in PI3Kδ (2.6 Å), and we realized that both co-structures were extremely similar (Fig. 18) despite one log difference in biochemical activity exhibited by (S)-**27** (Table 2) [79].

The two co-structures obtained were otherwise very consistent with those previously collected in the pyrimidinone series using PI3Kγ as a surrogate protein (e.g., Fig. 16a) and for other publicly reported propeller-shaped selective ligands [80]. With respect to PI3Kβ, key and common observations were interaction of the morpholine moiety with the hinge region via the main-chain nitrogen of Val848, movements of the P-loop Trp781 and Met773 opening a specific pocket where the indoline moiety stacks.

From these findings emerged the following paradoxes:

1. A similar conformational change can occur across the different PI3K isoforms to create a specific pocket.
2. Biochemically inactive but propeller-shaped molecules can co-crystallize in PI3Ks and occupy the so-called selectivity pocket.
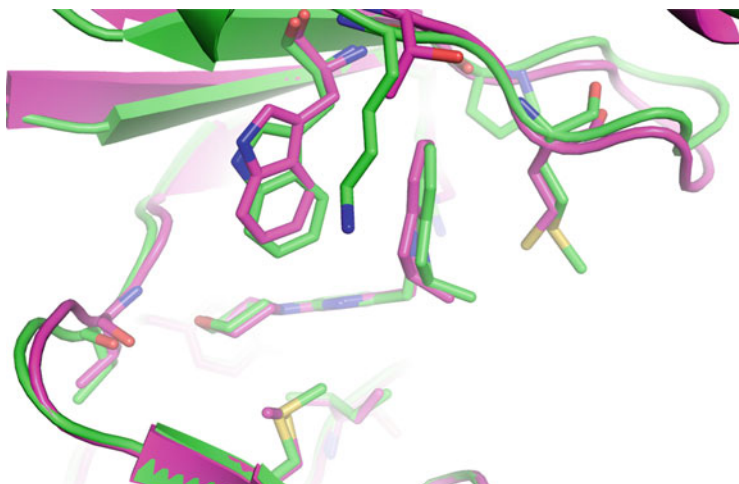
Fig. 18 3D-structure overlay of compound **(S)-27** co-crystallized in PI3Kβ vs PI3Kδ
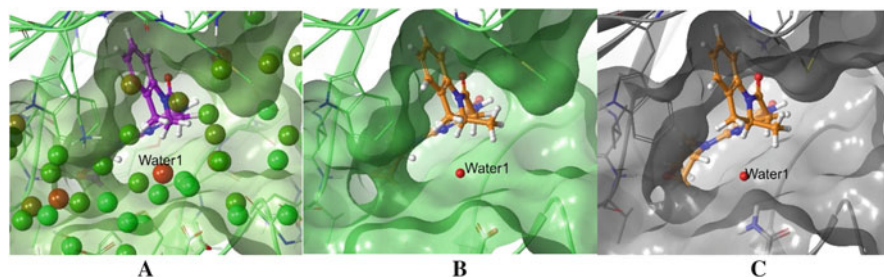

**Fig. 19** (**a**) **24** in PI3Kβ. (**b**) **(S)-27** in PI3Kβ. (**c**) **(S)-27** in PI3Kδ

3. All the selectivity pocket residues in interaction with the propeller-shaped ligand are extremely conserved across the PI3K isoforms.

To tentatively rationalize at least the unintuitive observed selectivity profile of (S)-**27** vs (R)-**27**, we further explored the two 3D co-structures collected with (S)-**27** in PI3Kβ and PI3Kδ and embarked in molecular dynamics simulations, solvent clustering, and statistical thermodynamic analysis using the WaterMap methodology [81] in order to investigate the network of water molecules at the vicinity of the ligand (<7 Å) and assess their respective entropy, enthalpy, and free energies [82]. With this algorithm, regions of high water density are identified as "hydration sites," and their corresponding enthalpies and entropies are computed relative to bulk solvent using inhomogeneous solvation theory.

Using WaterMap calculations, a large number of water molecules were predicted to be present around the non-methylated ligand **24** (Fig. 19a), but one drew our attention as it was associated with high positive free energy (+6.0 kcal/mol) and

Table 3 Calculated free energies of binding in kcal/mol relative to **24** with WaterMap (WM)

Compound	$\Delta\Delta G$ WM PI3Kβ	$\Delta\Delta G$ WM PI3Kδ
(S)-**27**	−0.04	0.84
(R)-**27**	−0.45	−3.59
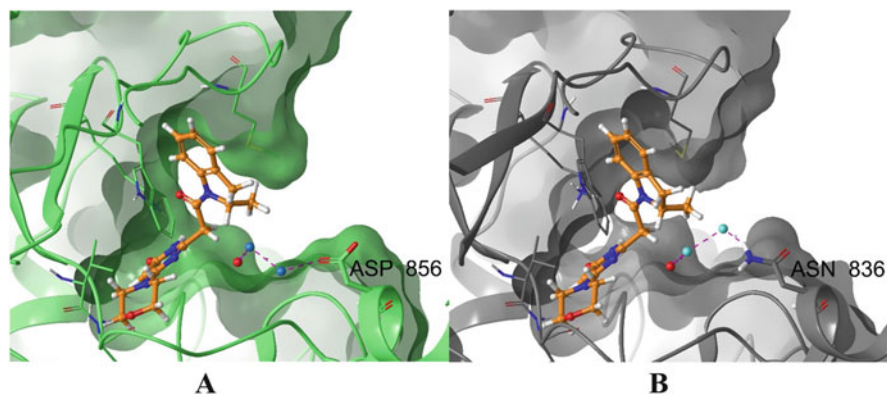
Fig. 20 Results of watermap calculations performed with (S)-27 bound to PI3Kβ (A) and PI3Kδ (B). Hydrogen-bond network through water molecules (blue spheres) between Water1 (red sphere) and ASP856 (in PI3Kβ) or ASN836 (PI3Kδ) is depicted as magenta dashed lines

therefore considered highly unstable [83]. Interestingly, this water molecule (that we will call Water1) was computed to be located in proximity to the 2-position of the indoline core and equi-energetically present in PI3Kδ (+5.8 kcal/mol). Visual inspection of the 3D structure established by WaterMap suggested that any substituent in the indoline 2-position with R or "down" stereochemistry would be perfectly suited for displacing Water1 leading to gain in free energy of ligand binding. WaterMap calculations with (S)-**27** recapitulated the same observation as for **24**; an unstable water molecule (Water1) is trapped by the (S)-ligand in the active site (Fig. 19b) decreasing its affinity (ΔG) vs the (R)-enantiomer which displaces it (Table 3). To reinforce the validity of this hypothesis, it is worth mentioning that computed free energies of binding were aligned in trends with the experimental ITC values collected (data not shown) not only for **24** and **27** but for a series of 2-substituted indoline analogs [83].

When applied to PI3Kδ, Water1 was not only retrieved but also estimated to be even more instable (+6.7 kcal/mol vs +5.9 kcal/mol in the case of **(S)-27**). However, the respective free energy values are too similar to quantitatively explain the observed selectivity pattern of the two enantiomers. A favorable displacement of the water molecule in PI3Kδ compared to PI3kβ cannot solely explain why **(R)-27** is more potent and less selective.

To better assess the origin of this selectivity pattern, binding site water molecules and nearby residues in both PI3Kβ and PI3Kδ were further analyzed. Water network originating from the unstable water molecule leads to a pair of residues that differ between the two isoforms. In PI3Kβ, Asp856 is connected to Water 1 through a

series of intermediate water molecules (Fig. 20a), whereas in PI3Kδ, the equivalent residue is Asn836, which is also located at ∼7 Å from the ligand and connected to Water1 via a similar network (Fig. 20b). Due to a more efficient charge transfer realized with Asp856 compared to the neutral Asn836, translated into more H-bonds to Water1, and shortest distances within the water network, PI3Kβ better tolerates the destabilizing influences of the methyl group in the (S)-configuration than PI3Kδ, which encloses Water1 in a more hydrophobic environment, leading to the observed selectivity. Interestingly, this hypothesis reconnects to the privileged residue analysis [23] as Asp856 is one of them.

Compound (S)-**27** became eventually SAR301260, a clinical development candidate tested in PTEN-deficient cancer patients [84].

6 Conclusions

Through the aforementioned projects which have been described, it was possible to identify and design very selective kinase inhibitors and dial out off-target affinity vs close kinase neighbors. If state-of-the art technologies were applied during the course of those projects (in biophysics, in modeling, etc.), serendipity in screens or in chemistry remained a significant contributor to these successful drug discovery programs. Moreover, exquisite selectivity was in certain circumstances rationalized a posteriori rather than guided (e.g., PI3Kβ). Still, the key protein elements or ligand properties which were identified to obtain and improve selectivity in one case or another have served subsequent kinase projects in our group and knowledge increased by experience for better efficiency. It is worth mentioning that other types of mechanisms of inhibition than acting directly in the conserved ATP cleft have been rarely explored or exploited in the kinase area [85, 86]. Only few kinases exhibit a true allosteric site (e.g., ABL) which could have been targeted to design a more specific generation of kinases inhibitors. In addition, to the best of our knowledge, approaches which were based on protein-protein interactions inhibition have failed to afford potent inhibitors except in the case of Akt [87]. Further investigations in new assay developments for hit-finding based, for example, on protein conformation changes [88] or in silico calculations to detect potential additional binding sites [89], should open new avenues for selective and specific kinase inhibitor discovery and development.

References

1. Manning G, Whyte DB, Martinez R, Hunter T, Sudarsanam S (2002) The protein kinase complement of the human genome. Science 298:1912–1934
2. Roskoski R (2018) FDA-approved protein kinase inhibitors. http://www.brimr.org/PKI/PKIs.htm
3. Monoclonal antibodies approved by the EMA and FDA for therapeutic use. http://www.actip.org/products/monoclonal-antibodies-approved-by-the-ema-and-fda-for-therapeutic-use/
4. Giordano S (2008) Curr Med Chem 15:422–432
5. Serrano C, George S (2014) Recent advances in the treatment of gastrointestinal stromal tumors. Ther Adv Med Oncol 6:115–127
6. Yan L, Rosen N, Arteaga C (2011) Targeted cancer therapies. Chin J Cancer 30:1–4
7. Jänne PA, Gray N, Settleman J (2009) Factors underlying sensitivity of cancers to small-molecule kinase inhibitors. Nat Rev Drug Discov 8:709–723
8. Knight ZA, Shokat KM (2005) Features of selective kinase inhibitors. Chem Biol 12:621–637
9. Schwartz PA, Murray BW (2011) Protein kinase biochemistry and drug discovery. Bioorg Chem 39:192–210
10. Morphy R (2010) Selectively nonselective kinase inhibition: striking the right balance. J Med Chem 53:1413–1437
11. Zhao Y, Adjei AA (2014) The clinical development of MEK inhibitors. Nat Rev Clin Oncol 11:385–400
12. Vogelstein B, Papadopoulos N, Velculescu VE, Zhou S, Diaz Jr LA, Kinzler KW (2013) Cancer genome landscapes. Science 339:1546–1558
13. Sullivan I, Planchard D (2017) Next-generation EGFR tyrosine kinase inhibitors for treating EGFR-mutant lung Cancer beyond first line. Front Med. https://doi.org/10.3389/fmed.2016.00076
14. Holderfield M, Deuker MM, McCormick F, McMahon M (2014) Targeting RAF kinases for cancer therapy: BRAF mutated melanoma and beyond. Nat Rev Cancer 14:455–467
15. Knighton DR et al (1991) Crystal structure of the catalytic subunit of cyclic adenosine monophosphate-dependent protein kinase. Science 253:407–414
16. Kornev AP, Haste NM, Taylor SS, Ten Eyck LF (2006) Surface comparison of active and inactive protein kinases identifies a conserved activation mechanism. PNAS 103:17783–17788
17. McClendona CL, Kornevc AP, Gilsonb M, Taylor SS (2014) Dynamic architecture of a protein kinase. PNAS 111:E4623–E4631
18. Brewer MR, Yun CH, Lai D, Lemmon MA, Eck MJ, Pao W (2013) Mechanism for activation of mutated epidermal growth factor receptors in lung cancer. PNAS 110:E3595–E3604
19. Fratev FF, Jónsdóttir SO (2009) An *in silico* study of the molecular basis of B-RAF activation and conformational stability. BMC Struct Biol 9:1–17
20. Echeverria I, Liu Y, Gabelli SB, Amzel LM (2015) Oncogenic mutations weaken the interactions that stabilize the p110a-p85a heterodimer in phosphatidylinositol 3-kinase α. FEBS J 282:3528–3542
21. Peng W, Thomas EN, Mads HC (2015) FDA-approved small-molecule kinase inhibitors. Trends Pharmacol Sci 36:422–439
22. Wu P, Nielsen TE, Clausen MH (2016) Small-molecule kinase inhibitors: an analysis of FDA-approved drugs. Drug Discov Today 21:5–10
23. Martin E, Mukherjee P (2012) Kinase-kernel models: accurate in silico screening of 4 million compounds across the entire human kinome. J Chem Inf Model 52:156–170
24. Taylor SS, Kornev PA (2011) Protein kinases: evolution of dynamic regulatory proteins. Trends Biochem Sci 36:65–77
25. Zarrinkar PP et al (2008) A quantitative analysis of kinase inhibitor selectivity. Nat Biotech 26:127–132

26. Jacobs MD, Caron PR, Hare BJ (2008) Classifying protein kinase structures guides use of ligand-selectivity profiles to predict inactive conformations: structure of lck/imatinib complex. Proteins 70:1451–1460
27. Zarrinkar PP et al (2011) Comprehensive analysis of kinase inhibitor selectivity. Nat Biotech 29:1046–1051
28. Fabbro D, Cowan-Jacob SW, Moebitz H (2015) Ten things you should know about protein kinases. Br J Pharmacol 172:2675–2700
29. Palmieri L, Rastelli G (2013) αC helix displacement as a general approach for allosteric modulation of protein kinases. Drug Discov Today 18:407–414
30. Gilmer TM (2008) Impact of common epidermal growth factor receptor and HER2 variants on receptor activity and inhibition by Lapatinib. Cancer Res 68:571–579
31. Hochegger H, Hegarat N, Pereira-Leal JB (2013) Aurora at the pole and equator: overlapping functions of Aurora kinases in the mitotic spindle. Open Biol. https://doi.org/10.1098/rsob.120185
32. Saya H (2002) Roles of aurora A kinase in mitotic entry and G2 checkpoint in mammalian cells. Genes Cells 7:1173–1182
33. Lampson MA, Cheeseman IM (2011) Sensing centromere tension: aurora B and the regulation of kinetochore function. Trends Cell Biol 21:133–140
34. Quartuccio SM, Schindler K (2015) Functions of Aurora kinase C in meiosis and cancer. Front Cell Dev Biol. https://doi.org/10.3389/fcell.2015.00050
35. Katayama H, Brinkley WR, Sen S (2003) The Aurora kinases: role in cell transformation and tumorigenesis. Cancer Metastasis Rev 22:451–464
36. Goldenson B, Crispino JD (2015) The aurora kinases in cell cycle and leukemia. Oncogene 34:537–545
37. Tang A, Gao K, Chu L, Zhang R, Yang J, Zheng J (2017) Aurora kinases: novel therapy targets in cancers. Oncotarget 8(14):23937–23954
38. Keen N, Taylor S (2004) Aurora-kinase inhibitors as anticancer agents. Nat Rev Cancer 4:927–936
39. Carry JC, Clerc F, Minoux H et al (2015) SAR156497, an exquisitely selective inhibitor of aurora kinases. J Med Chem 58:362–375
40. Roskoski R (2016) Classification of small molecule protein kinase inhibitors based upon the structures of their drug-enzyme complexes. Pharmacol Res 103:26–48
41. Tong M, Seeliger MA (2015) Targeting conformational plasticity of protein kinases. ACS Chem Biol 10:190–200
42. Organ SL, Tsao MS (2011) An overview of the c-MET signaling pathway. Ther Adv Med Oncol 3(1 Suppl):S7–S19
43. Zhang J, Babic A (2016) Regulation of the MET oncogene: molecular mechanisms. Carcinogenesis 37:345–355
44. Tovar EA, Graveel CR (2017) MET in human cancer: germline and somatic mutations. Ann Trans Med 5(10):205. https://doi.org/10.21037/atm.2017.03.64
45. Dixit A, Torkamani A, Schork NJ, Verkhivker G (2009) Computational modeling of structurally conserved cancer mutations in the RET and MET kinases: the impact on protein structure, dynamics, and stability. Biophys J 96:858–874
46. Xu J, Wang J, Zhang S (2017) Mechanisms of resistance to irreversible epidermal growth factor receptor tyrosine kinase inhibitors and therapeutic strategies in non-small cell lung cancer. Oncotarget 8(52):90557–90578
47. Soria JC et al (2012) *ALK* translocation and crizotinib in non-small cell lung cancer: an evolving paradigm in oncology drug development. Eur J Cancer 48:961–973
48. Mo HN, Liu P (2017) Targeting *MET* in cancer therapy. Chronic Dis Trans Med 3(3):148–153
49. Schio L, Nemecek C, Ugolini T et al (2012) SAR125844: a potent and selective ATP-competitive inhibitor of MET kinase. Cancer Res 72(8, Suppl.1):2911
50. Schio L et al (2016) Discovery, pharmacokinetic and pharmacological properties of the potent and selective MET kinase inhibitor, 1-{6-[6-(4-Fluoro-phenyl)-[1,2,4]triazolo[4,3-b]pyridazin-

3-ylsulfanyl]-benzothiazol-2-yl}-3-(2-morpholin-4-yl-ethyl)-urea (SAR125844) J. Med Chem 59:7066–7074

51. Romano G, Giordano A (2008) Role of the cyclin-dependent kinase 9-related pathway in mammalian gene expression and human diseases. Cell Cycle 7(23):3664–3668

52. Dussault I, Bellon SF (2009) From concept to reality: the long road to c-met and RON receptor tyrosine kinase inhibitors for the treatment of Cancer. Anti Cancer Agents Med Chem 9:221–229

53. Komoto J, Yamada T, Takata Y, Markham GD, Takusagawa F (2004) Crystal structure of the S-Adenosylmethionine Synthetase ternary complex: a novel catalytic mechanism of S-Adenosylmethionine synthesis from ATP and met. Biochemistry 43:1821–1831

54. Eathiraj S et al (2011) Discovery of a novel mode of protein kinase inhibition characterized by the mechanism of inhibition of human Mesenchymal-epithelial transition factor (c-met) protein autophosphorylation by ARQ 197. J Biol Chem 286(23):20666–20676

55. Coumaran E, Goulaouic H (2015) Selective intravenous inhibitor of the MET tyrosine kinase SAR125844 inhibits tumor growth in MET-amplified Cancer. Mol Cancer Ther 14(2):384–394

56. Angevin E et al (2017) A first-in-human phase I study of SAR125844, a selective MET tyrosine kinase inhibitor, in patients with advanced solid tumours with MET amplification. Eur J Cancer 87:131–139

57. Lindmo K, Stenmark H (2006) Regulation of membrane traffic by phosphoinositide 3-kinases. J Cell Sci 119:605–614

58. Backer JM (2016) The intricate regulation and complex functions of the class III phosphoinositide 3-kinase Vps34. Biochem J 473(15):2251–2271

59. Stjepanovic G, Baskaran S, Mary G, Lin MG, Hurley JH (2017) Unveiling the role of VPS34 kinase domain dynamics in regulation of the autophagic PI3K complex. Mol Cell Oncol 4(6): e1367873

60. Bilanges B (2017) Vps34 PI3-kinase inactivation enhances insulin sensitivity through reprogramming of mitochondrial metabolism. Nat Commun 8(1):1804. https://doi.org/10.1038/s41467-017-01969-4

61. Honda A et al (2016) Potent, selective, and orally bioavailable inhibitors of VPS34 provide chemical tools to modulate autophagy in vivo. ACS Med Chem Lett 7:72–76

62. Pasquier B (2016) Autophagy inhibitors. Cell Mol Life Sci 73:985–1001

63. Peppard JV, Ronan B, Pasquier B (2014) Identifying small molecules which inhibit autophagy: a phenotypic screen using image-based high-content cell analysis. Curr Chem Genom Trans Med 8(Suppl-1, M2):3–15

64. Pasquier B, El-Ahmad Y, Filoche-Rommé B et al (2015) Discovery of (2S)-8-[(3R)-3-Methylmorpholin-4-yl]-1-(3-methyl-2-oxobutyl)-2-(trifluoromethyl)-3,4-dihydro-2Hpyrimido [1,2-a]pyrimidin-6-one: a novel potent and selective inhibitor of Vps34 for the treatment of solid tumors. J Med Chem 58:376–400

65. Pasquier B, Goulaouic H et al (2014) A highly potent and selective Vps34 inhibitor alters vesicle trafficking and autophagy. Nat Chem Biol 10:1013–1019

66. Pasquier B (2015) SAR405, a PIK3C3/Vps34 inhibitor that prevents autophagy and synergizes with mTOR inhibition in tumor cells. Autophagy 11(4):725–726

67. Kriplani N, Hermida MA, Brown ER, Leslie NR (2015) Class I PI3-kinases: function and evolution. Adv Biol Regulation 59:53–64

68. Vadas O, Burke JE, Zhang X, Berndt A, Williams RL (2011) Structural basis for activation and inhibition of class I Phosphoinositide 3-kinases. Sci Signal 4(195):re2

69. Yu JSL, Cui W (2016) Proliferation, survival and metabolism: the role of PI3K/AKT/mTOR signaling in pluripotency and cell fate determination. Development 143:3050–3060

70. Millis SZ, Ikeda S, Reddy S, Gatalica Z, Kurzrock R (2016) Landscape of Phosphatidylinositol-3-kinase pathway alterations across 19784 diverse solid tumors. JAMA Oncol 2(12):1565–1573

71. Lengauer C et al (2008) PTEN-deficient cancers depend on PIK3CB. Proc Natl Acad Sci U S A 105(35):13057–13062

72. Dillon LM, Miller TW (2014) Therapeutic targeting of cancers with loss of PTEN function. Curr Drug Targets 15(1):65–79
73. Greenwell IB, Ip A, Cohen JB (2017) PI3K inhibitors: understanding toxicity mechanisms and management. Oncology (Williston Park) 31(11):821–828
74. Williams RL (2011) Structure of lipid kinase p110b/p85b elucidates an unusual SH2-domain-mediated inhibitory mechanism. Mol Cell 41:567–578
75. Metz A, Ciglia E, Gohlke H (2012) Modulating protein-protein interactions: from structural determinants of binding to Druggability prediction to application. Curr Pharm Des 18:4630–4647
76. Vlahos CJ, Matter WF, Hui KY, Brown RF (1994) A specific inhibitor of phosphatidylinositol 3 kinase, 2-(4-Morpholinyl)-8-phenyl-4H-l-benzopyran-4-one (LY294002). J Biol Chem 269 (7):5241–5248
77. Certal V, Halley F, Virone-Oddos A et al (2012) Discovery and optimization of new benzimidazole- and benzoxazole-pyrimidone selective PI3Kβ inhibitors for the treatment of phosphatase and TENsin homologue (PTEN)-deficient cancers. J Med Chem 55:4788–4805
78. Knight ZA, Williams RL, Shokat KM (2006) A pharmacological map of the PI3-K family defines a role for p110α in insulin signaling. Cell 125(4):733–747
79. Certal V, Carry JC, Frank Halley F et al (2014) Discovery and optimization of pyrimidone indoline amide PI3Kβ inhibitors for the treatment of phosphatase and Tensin homologue (PTEN)-deficient cancers. J Med Chem 57:903–992
80. Somoza JR et al (2015) Structural, biochemical, and biophysical characterization of Idelalisib binding to Phosphoinositide 3-kinase δ. JBC 290(13):8439–8446
81. Robinson DD. WaterMap – theory and practical applications. http://content.schrodinger.com/Training+Material/WM/Hsp90/WaterMap-orig.pdf
82. Wang L, Berne BJ, Friesner RA (2011) Ligand binding to protein-binding pockets with wet and dry regions. PNAS 108(4):1326–1330
83. Robinson D, Bertrand T, Carry JC et al (2016) Differential water thermodynamics determine PI3K-Beta/Delta selectivity for solvent-exposed ligand modifications. J Chem Inf Model 56:886–894
84. Demers B et al (2018) First-in-human trial of the PI3Kβ-selective inhibitor SAR260301 in patients with advanced solid tumors. Cancer 124(2):315–324
85. Wu P, Clausen MH, Nielsen TE (2015) Allosteric small-molecule kinase inhibitors. Pharmacol Ther 156:59–68
86. Cowan-Jacob SW, Jahnke W, Knapp S (2014) Novel approaches for targeting kinases: allosteric inhibition, allosteric activation and pseudokinases. Future Med Chem 6(5):541–561
87. Cheng Y et al (2012) MK-2206, a novel allosteric inhibitor of Akt, synergizes with gefitinib against malignant glioma via modulating both autophagy and apoptosis. Mol Cancer Ther 11 (1):154–164
88. Simard JR, Rauh R (2014) FLiK: a direct-binding assay for the identification and kinetic characterization of stabilizers of inactive kinase conformations. Methods Enzymol 548:147–171
89. Leis S, Schneider S, Zacharias M (2010) In Silico prediction of binding sites on proteins. Curr Med Chem 17:1550–1562